CHAPTER 148

SEDIMENT TRANSPORT OVER RIPPLES IN WAVES AND CURRENT

G. Perrier[1-3], E.A. Hansen[2], C. Villaret[3], R. Deigaard[1] and J. Fredsøe[1]

ABSTRACT

Numerical simulations are presented for the flow and the dynamics of non-cohesive sediment over 2D ripples in waves and current. For this purpose, a model based on a discrete vortex approach using the "cloud-in-cell" concept has been applied. The hydrodynamic model drives a Lagrangian model for the suspended sediment.

The characteristic vorticity structures prevailing in the vicinity of ripples are accurately replicated and sediment suspension mechanisms are successfully described. Thus, the sediment transport resulting from asymmetrical waves and combined waves and current can be predicted. Especially, the wave-related component of the transport opposes the maximum free stream velocity and contributes significantly to the total transport. In the present work, the effect of the wave-induced drift is not included.

INTRODUCTION

A detailed understanding of flow kinematics and suspension mechanisms of non-cohesive sediments in waves and current situations is of great interest to coastal engineers because of its importance in sediment transport predictions.

When the seabed is plane, the suspension of sediment is governed by turbulent diffusion. But when ripples occur on the bed, the prevailing process becomes convection. At each half-cycle of the oscillation, coherent vorticity structures are formed in the lee side of the ripple and trap sediment. At flow reversal, these sediment laden vortices are shed into the flow, thus giving rise to suspension.

In the field of non breaking regular waves, experimental investigations have been conducted for flows over 2D ripples (Sato *et al*, 1984; Ranasoma and Sleath, 1992). In connection with the hydrodynamics, experimenters have studied sediment dynamics (Sleath, 1982). For asymmetrical waves, few experiments exist (Sato and Horikawa, 1986). For combined waves and current flows, whereas comprehensive experiments over flat beds are rather numerous, fewer are available for rippled beds (Murray, 1992; Villaret and Latteux, 1992).

[1] *ISVA, Building 115, Technical University of Denmark, DK 2800 Lyngby, Denmark*
[2] *Danish Hydraulic Institute, Agern Allé 5, DK 2970 Hørsholm, Denmark*
[3] *Laboratoire National d'Hydraulique, 6 Quai Watier 78401 Chatou, France*

To model the flow over ripples, different methods have been developed : vorticity-stream function formulation with finite difference and spectral methods (Blondeaux and Vittori, 1990), classical turbulence models : K-ε (Tsujimoto *et al*, 1991), or K-L (Huynh Thanh, 1990), and discrete vortex methods by Longuet-Higgins (1981), Block (1994) and Hansen *et al* (1994).

To model sediment suspension, the common approach is based on the turbulent diffusion equation where the sediment diffusivity relies on various assumptions (Fredsøe and Deigaard, 1992). Nevertheless, in the case of rippled beds, convection becomes the prevailing process. The diffusion assumption has been used by Tsujimoto (1991) coupled with his K-ε model, but most of the other models are based on a Lagrangian particle tracking (Blondeaux and Vittori, 1990; Block, 1994; Hansen *et al*, 1994).

In this study, a discrete vortex approach is adopted to achieve a 2D model for the flow, the sediment suspension mechanisms and the resulting net transport. After a brief presentation of the model, hydrodynamic calculations are performed for an oscillatory flow over fixed ripples. Then, the complete model is used to study the asymmetrical wave case and the combined sine waves and current case. Experimental conditions are listed in appendix.

PRESENTATION OF THE DISCRETE VORTEX MODEL

The discrete vortex model (DVM) developed by ISVA-DHI is designed to compute complex instationary flows interacting with structures or stationary seabeds. The model relies on a discretization of vorticity in "vortices" and concentration in "particles" combined with a finite difference method. A detailed description is presented in Hansen *et al* (1994).

The hydrodynamical model.

The model is based on a vorticity-stream function formulation:

Poisson equation : $$\nabla^2\psi=-\omega \qquad [1]$$

Vorticity transport equation : $$\frac{d\omega}{dt}=\nu\nabla^2\omega \qquad [2]$$

(ψ is the stream function, ω the vorticity and ν the kinematic viscosity).

Using an operator splitting method, the vorticity transport equation [2] is split into :

a convection equation : $$\frac{\partial\omega}{\partial t}+u\frac{\partial\omega}{\partial x}+v\frac{\partial\omega}{\partial y}=0 \qquad [3]$$

and a diffusion equation : $$\frac{\partial\omega}{\partial t}=\nu\nabla^2\omega \qquad [4]$$

The convective transport is then modelled by moving the individual vortices with the velocity field (u,v), while the diffusive transport is described by adopting a random walk technique : at each time step Δt, vortices are moved with a random displacement following a Gaussian distribution characterised by the standard deviation :

$$\sigma=\sqrt{2\nu\Delta t} \qquad [5]$$

The Poisson equation [1] is solved on a curvilinear finite difference grid by an Alternative Direction Implicit method. The grid is generated from a solution to the Laplace equation describing a periodic potential flow over ripples.

Cloud-in-cell technique.

To obtain the vorticity field from the set of vortices, a cloud-in-cell technique is used to distribute the circulation of the vortices in each cell as vorticity on the four grid points at the cell corners.

Boundary layer model at the surface.

Vorticity can only be generated by shear forces acting on physical surfaces. On these boundaries, a turbulent boundary layer model based on the integrated momentum equation (Fredsøe, 1984) gives the time development of the boundary layer and hence, determine the strength and the motion of vortices within this zone.

Merging method.

To limit the growth of the number of vortices and to get a feasible calculation, a merging procedure is introduced : when two vortices with opposite signs come closer to each other than the sum of their radii, they combined into one single vortex.

Computational domain and boundary conditions.

In the computations, the bed is assumed stationary and a time-independent domain is used. In most of the presented simulations, the horizontal length of the domain is two ripple lengths. Vertically, various discretizations have been used. For the wave-alone case, where the vorticity is confined in the near-bed layer, a stretched net is adopted, with a height chosen so that vortices do not reach the top boundary. In the wave-current case, the boundary layer develops over the entire depth. As non-physical boundaries are difficult to represent in this kind of model, a symmetrical domain with ripples at the top has been chosen in order to satisfy the symmetry condition on the center line. In some facilities such as shallow tunnels, a real domain covering the entire depth can be used.

No-slip conditions are applied on physical boundaries while a simple stream line condition (ψ=constant) is used at the top for the wave-alone case. To drive the flow, the time-dependent water discharge is imposed via the stream function. Besides, spatial periodicity between the two lateral boundaries is prescribed.

The sediment transport model.

The total sediment transport is divided into two contributions : bed load and suspended load. In the present model, it is assumed that the ripple shape is stationary and that the presence of suspended sediment does not affect the hydrodynamics. The two components of the sediment transport are modelled as follows.

* The bed load transport rate Q_b along the ripple is modelled with the Meyer-Peter and Müller formula corrected for the slope effect :

$$\frac{Q_b}{\sqrt{(s-1)gd_{50}^3}} = 8\left[\theta-\theta_c\left(1+\frac{1}{\tan\varphi}\frac{dy_b}{dx_b}\right)\right]^{3/2} \qquad [6]$$

where θ is the local instantaneous Shields parameter, θ_c the critical Shields parameter, s the relative density of the sediment, g the gravity, φ the angle of repose of the sediment, d_{50} the mean grain diameter and (x_b,y_b) are the bed coordinates.

* The suspended sediment is discretized in computational "particles" containing a certain amount of sediment. They are characterised by their mass and their fall velocity.

The generation of these particles at the ripple surface involves two different mechanisms :

- The action of shear stresses on the bed produces a local erosion and thus creates new suspended particles. To model this, a source of sediment is located at the level $y^*_o=2d_{50}$ (y^* is the coordinate normal to the ripple surface). Its strength Q_d is determined as a source term in the local turbulent diffusion equation in order to satisfy the bed-concentration formula of Zyserman and Fredsøe (1994) :

$$c_b(y^*_o=2d_{50})=\frac{0.331\,(\theta-0.045)^{1.75}}{1+\frac{0.331}{0.46}\,(\theta-0.045)^{1.75}} \qquad [7]$$

The mass of the particles is then derived from Q_d. To account for the grain sorting effect, the settling velocity is based on the mean grain diameter of the suspended fraction $d_{50,susp}$, fraction defined as sediment with a settling velocity $w_s < 0.8\ u_f$ where u_f is a characteristic friction velocity at the crest.

- Due to the recirculation zone downstream of the crest, the bed load is ejected into the flow at the separation point as described by Sleath (1982). This contribution is modelled by calculating Q_b at the location of maximum Shields parameter upstream of the separation. Then, a new particle is introduced just above the separation point with a mass derived from Q_b and a fall velocity based on the mean grain diameter of the bed material d_{50}.

Similarly to the hydrodynamic model, the continuity equation for the suspended sediment concentration [8] is tackled in a Lagrangian fashion.

$$\frac{dc}{dt}=w_s\frac{\partial c}{\partial y}+\nabla.(\varepsilon_s\nabla c) \qquad [8]$$

where c is the concentration, w_s the settling velocity and ε_s the sediment diffusivity. The motion of the sediment suspended over vortex ripples is dominated by convection except in the boundary layer along the ripple surface where the turbulent diffusion becomes important. Therefore, sediment particles are assumed to follow the flow paths with a fall component.
Inside the boundary layer, the motion normal to the ripple surface due to turbulent diffusion is modelled by a random walk method in the same manner as for the vorticity. Here, the standard deviation is :

$$\sigma_s=\sqrt{2\varepsilon_s\Delta t_s} \qquad [9]$$

where the sediment diffusivity ε_s is assumed to be equal to the eddy viscosity ν_t, which has a linear variation within the boundary layer :

$$\varepsilon_s=\nu_t=\kappa u_f y^* \qquad [10]$$

where u_f is the local instantaneous friction velocity given by the boundary layer model, κ is the Von Karman's constant and Δt_s is the time step for sediment typically much smaller than the hydrodynamical time step Δt.

Discretization parameters.

The computational grid presents 50 potential lines along a ripple length. The hydrodynamical time step is T/360 (where T is the wave period) and the sediment time step is $\Delta t_s=\Delta t/10$. Numerical independence of the solution has been tested.

Results processing.

After a transient regime of at least 20 cycles, any variable z(x,y,t) is decomposed into a mean (time-averaged) component Z, a periodic (phase-averaged) component z_w and a fluctuating component z'. Averaging is performed over at least 20 cycles :

$$z(x,y,t)=Z(x,y)+z_w(x,y,t)+z'(x,y,t) \quad [11]$$

Variables are then spatially averaged along horizontal lines with at least 50 points per ripple wave length. In the following angle brackets will denote space-averaged and an overbar or a capital time-averaged.
Assuming turbulent fluxes to remain small, the time and space averaged horizontal flux of suspended sediment, $F_s=\overline{<u(x,y,t)c(x,y,t)>}$ is found to be made of two components :

$$F_s=F_c+F_w \quad [12]$$

where $F_c=<U(x,y)><C(x,y)>$, the current flux, represents the advection of the mean concentration by the mean velocity and F_w, the wave flux comes out from the non-zero covariance between periodic components u_w and c_w. The model provides F_s and F_c, F_w is then obtained by subtraction.

To compute total suspended transport rates, two different methods can be used :
- Eulerian method : depth-integration of the fluxes profiles gives the transport rate Q_s and its two components Q_c and Q_w. This method is the one utilised in experiments. Particular attention must be paid to the lower integration limit and the large gradients in the near-bed region.
- Lagrangian method : the transport rate Q_s is directly computed from each "particle" contribution.
The total transport rate Q_t is the sum of the transport rate for the bed load and the transport rate for the suspended load calculated with the Lagrangian method :

$$Q_t=Q_b+Q_s \quad [13]$$

In the model, all the variables are made non-dimensional with the length scale L_r and the time scale L_r/U_w (where L_r is the ripple length and U_w the wave velocity amplitude). At the crest location x=0 and at mid ripple height y=0 whereas y_c denotes the vertical coordinate relative to the crest level. The positive direction (x>0) will refer as the direction of maximum free stream velocity. As only phase-averaged and time-averaged results will be presented throughout the paper, the notation z will be used for $Z+z_w$.

HYDRODYNAMIC COMPARISON

Detailed LDA velocity measurements were carried out by Ranasoma (92) over stabilised ripples fixed on a rig oscillating in a closed tank. The experiment covered various combinations of beds and oscillations. In the following, a comparison is presented for the selected test 2a with ripples in equilibrium with the flow. The ratio between wave orbital amplitude and ripple wave length $a/L_r=0.78$ is in the range of vortex ripples, or orbital ripples as classified by Wiberg and Harris (1994). The simulated ripple shape is averaged from the measured bed profile.
The initial time corresponds to maximum negative free stream velocity U_∞ relative to the bed as illustrated on figure 1.

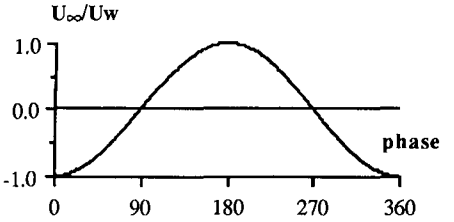

Fig. 1. Free stream velocity history. Experiment of Ranasoma (1992).

The agreement between computed and measured vorticity fields at two "key" phases demonstrates the ability of the hydrodynamic model to reproduce the important flow features. The vortex formation is well predicted (intensity, size and core location) whereas small differences appear before flow reversal : in the calculation, the core of the vortex appears closer to the crest and its spatial extent is larger. The convection and the decay of the ejected vortex agree with measurements, its location after one half-cycle is only slightly higher in the calculation : fig (2.1) shows the vortex shed one half-cycle before from the neighbouring ripple which is about to pass over the crest.

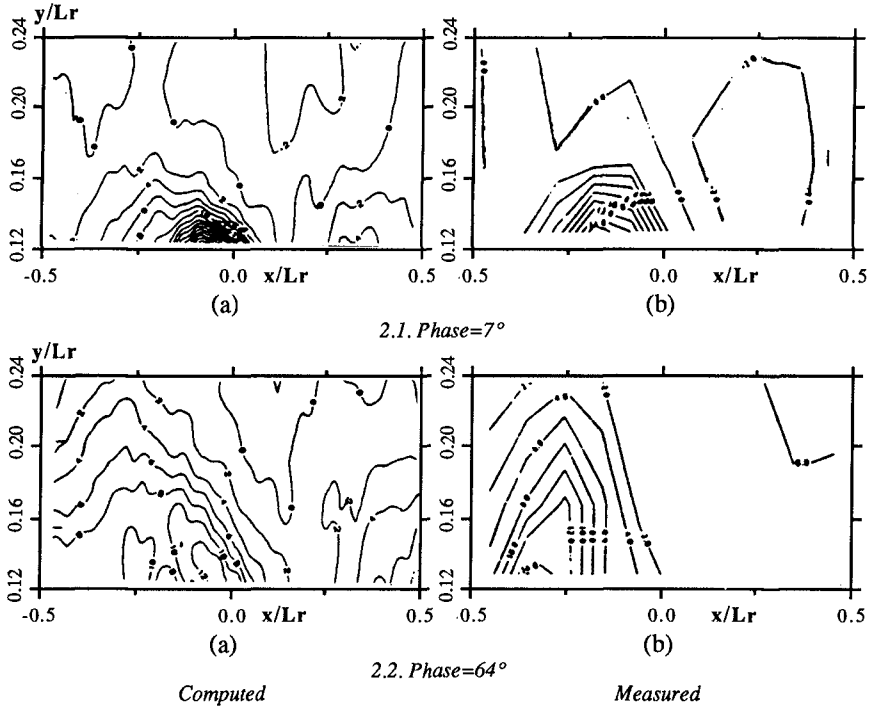

Fig. 2. Non-dimensional vorticity field at 2 phases. Experiment of Ranasoma (1992).

The time-evolution of the space-averaged horizontal defect velocity (velocity relative to the free stream) $\langle u_d(x,y,t)\rangle=\langle u(x,y,t)\rangle-U_\infty(t)$ and momentum $\langle u(x,y,t)v(x,y,t)\rangle$ is plotted on figure 3. The velocity amplitude is in good agreement close to the bottom (y_c=1mm) but the simulation assesses a slower decay with elevation, which is consistent with the higher location of vortices. There is a phase shift between computed and measured profiles close to the bottom (y_c=1mm) for velocity extrema. This is associated with the location of the vortex core closer to the crest in the simulation resulting in a slightly earlier "sweep" on the bed. The momentum curves exhibit three peaks per half-cycle, each peak connected to a particular flow structure as described by Ranasoma (1992) :

- Peak (1) : the vortex sweep close to flow reversal throws upwards accelerated fluid from the crest and brings down still fluid above the trough.
- Peak (2) : the vortex is now located in the trough. Its circulation carries up slow-moving fluid above the trough and brings down fast-moving fluid above the crest.
- Peak (3) : the vortex has arrived above the crest of the neighbouring ripple. The combined effects of the vortex circulation, the local spatial acceleration at the crest and the separation zone in formation bring up more positive momentum from the crest than bring down negative momentum above the trough.

The model fits well the general peak structure. The only significant discrepancies are observed for the peak (1) : it occurs slightly later in the simulation the amplitude is relatively larger.

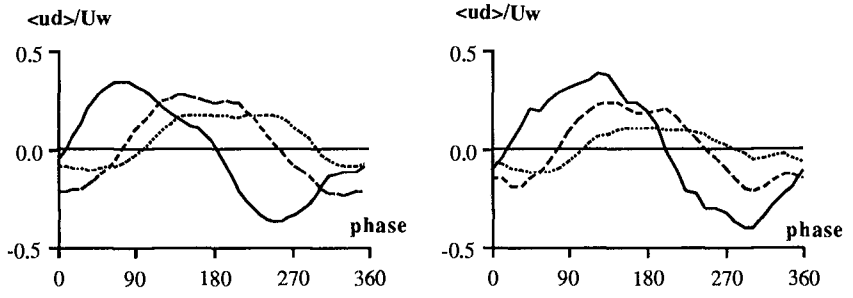

Computed *Measured*

Fig. 3.1. Space averaged non-dimensional defect horizontal velocity.
(solid : y_c=1mm; dashed : y_c=9mm; dotted : y_c=20mm). Experiment of Ranasoma (1992).

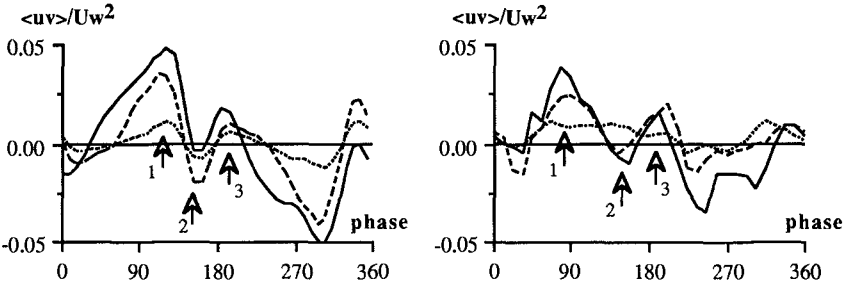

Computed *Measured*

Fig. 3.2. Space averaged non-dimensional momentum.
(solid : y_c=4mm; dashed : y_c=9mm; dotted : y_c=20mm). Experiment of Ranasoma (1992).

The hydrodynamical model appears to be in very good agreement with the experiment. The slight differences are not significant.

SEDIMENT TRANSPORT IN ASYMMETRICAL WAVES

A series of experiments in a water tunnel with a sandy bed under asymmetrical Stokes and cnoidal wave conditions have been carried out by Sato and Horikawa (1986).

In the following, the simulation of the selected test C2-12 is presented. In this test, the driving free stream velocity signal (Fig. 4) is based on a third-order cnoidal wave with an asymmetry parameter $U_w/\hat{U}=0.72$ and a zero time-averaged value. The ratio $a/L_r=1.3$ and the measured ripple is 2D with an asymmetry parameter $L_u/L_r=0.65$. The simulated ripple is "smoothed parabolic" : parabolically shaped troughs with a crest smoothed over 10 % (Fig. 5). The mean sand grain diameter is d_{50}= 0.18mm. As the height of the tunnel is only about twice the ripple length, it has been chosen to use the whole height as a computational domain taking a flat smooth boundary at the top.

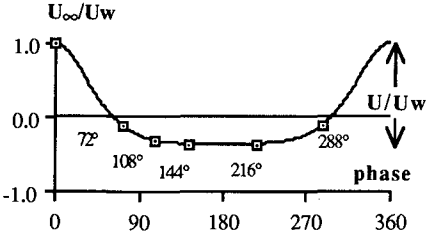

Fig. 4. Free stream velocity history.

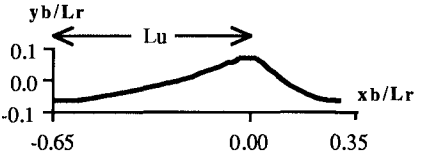

Fig. 5. Ripple shape.

Experiment of Sato and Horikawa (1986).

A snap-shot of the particles distribution is shown after flow reversal on figure (6) and the time evolution of the concentration field over a complete wave-cycle is displayed on figure (7) for 5 phases. On the steep flank of the ripple, a sand cloud forms with a large input of sediment from the crest during the short positive part of the cycle. At flow reversal, this cloud is ejected over the crest and travels in the negative direction. While convected, the cloud undergoes some diffusion and a large part of the trapped sediment falls down on the bed. During the longer negative part of the cycle, the flow motion is slow and no sand cloud formation is observed on the mild flank of the ripple, the friction velocity being too small and the slope too mild to get a sand cloud. Thus, a strong asymmetry exists between the two parts of the wave cycle resulting in a negative transport.

Fig. 6. Computed particles distribution at 108°. Experiment of Sato and Horikawa (1986).

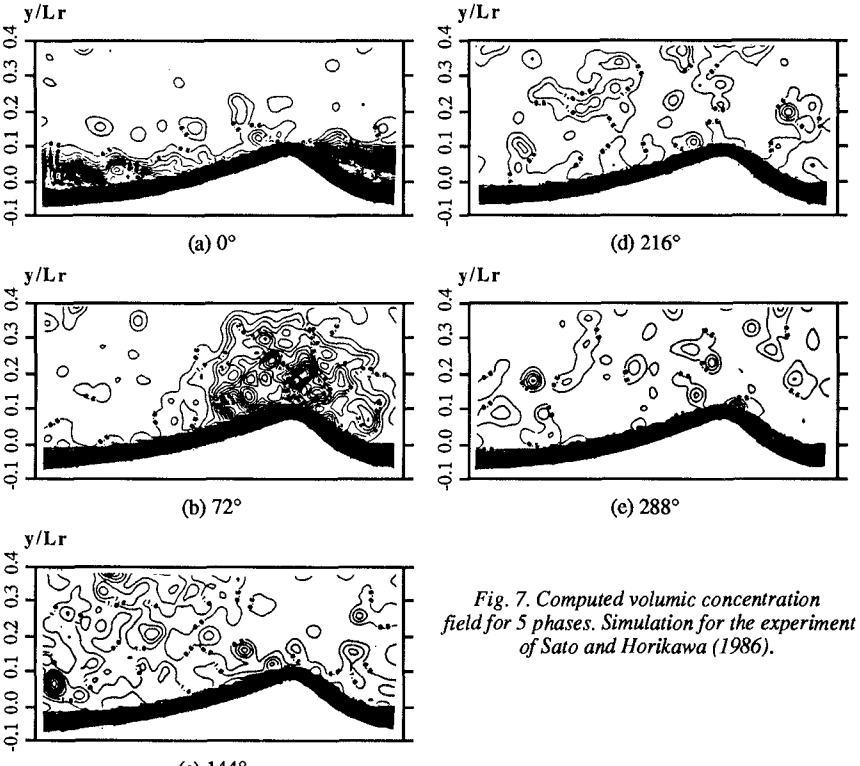

Fig. 7. Computed volumic concentration field for 5 phases. Simulation for the experiment of Sato and Horikawa (1986).

The computed horizontal suspended sediment fluxes (Fig. 8) reveal that the transport occurs only in a layer 0.5 L_r thick. Because of the return current in the bottom part, F_c is negative down to the crest level. The wave flux F_w is negative above the level $y_c = 0.06\ L_r \approx 0.4\ H_r$ (where H_r is the ripple height) as a result of sand cloud convection processes in this region and becomes positive below. The total suspended flux is then negative except very close to the bottom.

Three representative tests for 2D ripples have been used for simulations with an increasing degree of asymmetry and flow severity. The agreement (Table 1) is close with only a small underprediction for weaker flow conditions (S3-03).

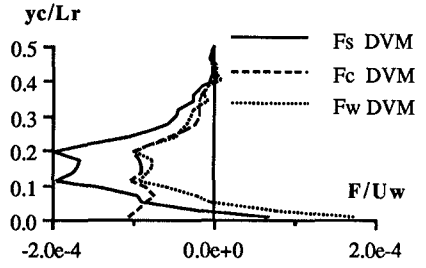

Fig. 8. Computed non-dimensional horizontal suspended sediment fluxes profiles. Experiment of Sato and Horikawa (1986).

Test	Qt/Lr/Uw *10^{-4}		
	DVM	***Exp***	***Ratio***
S3-03	-0.2	-0.5	0.4
C2-12	-1.0	-1.5	0.7
C3-37	-1.1	-1.4	0.8

Table 1. Non-dimensional net sediment transport rates. Experiment of Sato and Horikawa (1986).

SEDIMENT TRANSPORT IN COMBINED WAVES AND CURRENT

In the following, two different simulations for combined waves and current are presented : experiment of Murray (1992) in a tunnel and experiment of Villaret and Latteux (1992) in a wave flume. As far as sediment transport is concerned, wave flumes and tunnels are not totally equivalent. Indeed, in a flume the presence of a wave propagating in the positive direction induces vertical velocities and an horizontal drift positive at the bottom and negative in the outer flow. This effect that might change bottom processes is not included in the model.

The value of the proper free stream current U_c to prescribe is obtained by data fitting on the space and time averaged horizontal velocity profile.

Combined waves and current in a tunnel.

Murray used a set of various hydraulic conditions essentially in the sheet flow regime. However, one test (WCS1) presented a rippled bed. Here, the parameter a/L_r=6.57 is out of the range of classic vortex ripples and is classified as anorbital by Wiberg and Harris (1994) : the ripple shape does not depend on the wave orbital amplitude but rather on the grain diameter d_{50}. The measured ripple shape is more 3D than 2D with no asymmetry reported. In the model, we choose a symmetric "smoothed parabolic" shape as a first approximation. The sand is fine with a mean grain diameter d_{50}=0.14mm.

The time and space averaged horizontal velocity and concentration are shown on figure (9). The two-slope velocity profile is well reproduced with a break of slope at $y_c/L_r \approx 0.5$ and only a slight underprediction in the lower part. The concentration profile is correct both in terms of bottom concentration and slope. Very close to the bed, the model predicts an increase in the concentration but no data points are available at these lower levels. At high elevations, the small overestimation is not significant for such low concentrations.

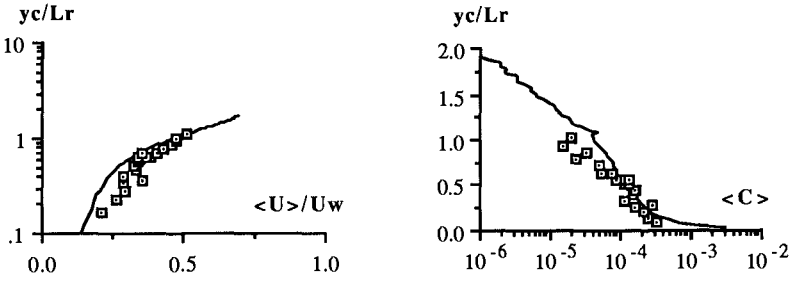

(a) Non-dimensional horizontal velocity. *(b) Volumic concentration.*

Fig. 9. Time and space averaged profiles.
solid line : DVM; squares: Experiment of Murray (1992)

The total suspended sediment flux profile F_s and the two contributions F_c and F_w presented on figure (10) appear to be in very good agreement with data. The strong reduction of the total flux by the negative wave contribution is properly predicted by the model at least above the level y_c/L_r=0.2. As we get closer to the bottom, current and wave contributions become strongly positive with a reversal of F_w at about one ripple height above the crest level. This behaviour has previously been observed by Vincent and Green (1990) for large scale ripples in the field.

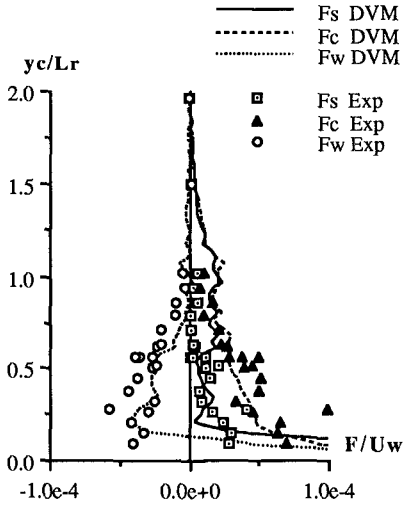

Fig. 10. Non-dimensional horizontal suspended sediment fluxes profiles. Experiment of Murray (1992).

$Q/L_r/U_w*10^{-5}$	*DVM*	*Exp*	*Ratio*
Bed load			
Q_b	0.5	*	*
Suspended load (Eul)			
Q_s	2.6	1.3	2.0
Q_c	3.9	4.1	0.9
Q_w	-1.3	-2.8	0.5
Suspended load (Lag)			
Q_s	7.0	*	*
Total load			
Q_t	7.5	*	*

Table 2. Non-dimensional transport rates. Experiment of Murray (1992). (: unavailable)*

To obtain transport rates, Murray used a linear extrapolation of the fluxes from the last measurement point (y_c/L_r=0.09) down to the averaged bed level (y=0) where F=0 and then performed a depth-integration. Table 2 shows that the same Eulerian method applied to model results gives an overprediction of Q_s by a factor 2. The current contribution Q_c agrees with data while the wave contribution Q_w is underpredicted. Once considered the shape of the flux F_w profile, the reason of the discrepancy is clearly the reversal for the lower levels. The Lagrangian method gives a larger (2.7 times) transport rate because it takes indirectly account of the very large positive transport beneath y_c/L_r=0.09. The proportion of bed load in the total load is predicted as only 6.6%.

Combined waves and current in a flume.

Villaret and Latteux (1992) have carried out combined waves and current experiments in a flume. For the selected test, the current followed the wave and the wave-induced drift is about 1 or 2 cm/s at the bottom for a velocity amplitude U_w=34 cm/s. The other differences with the previous tunnel experiment are a larger current : U_{c1}/U_w=1.0 for Villaret and Latteux (1992) whereas U_{c1}/U_w=0.5 for Murray (1992) (U_{c1} is the current at y_c/L_r=1.0), a finer sand (d_{50}=0.09mm) and a smaller ratio a/L_r=1.9, at the upper range of the vortex ripples regime and classified as suborbital by Wiberg and Harris (1994). The ripple was 2D but no asymmetry was reported. In the model, we use a symmetric "smoothed parabolic" shape.

The computed horizontal velocity deviates significantly from data (Fig. 11.a.). The model exhibits a two-slope profile with a break of slope at y/L_r=0.5 and a larger apparent roughness with even negative velocity in the near-bed wave-current boundary layer where data shows rather large positive velocities. The discrepancy at the bottom is a result of the wave drift present in the experiment but not included in the simulation.

In contrast with flat beds, the increase in the current-wave ratio U_c/U_w from the simulation of Murray (1992) to Villaret and Latteux (1992) results in a larger apparent roughness. Actually, the regime is closer to vortex ripples and the flow asymmetry is larger. Hence, shed vortices strongly reduce the velocity.

In spite of the correct bottom concentration, the calculated profile appears too steep in its lower part (Fig. 11.b.). The two-layer structure is rather pronounced attesting the large-scale mixing in the lower layer dominated by vortex convection.

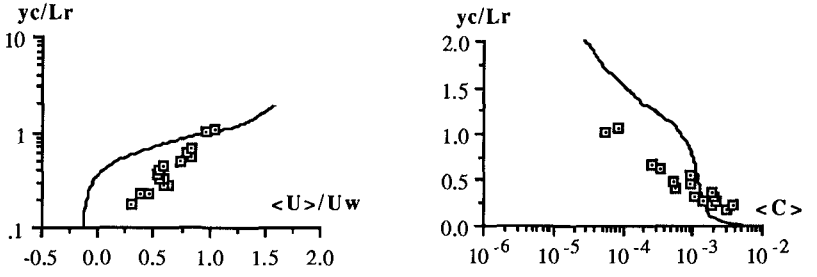

(a) Non-dimensional horizontal velocity. (b) Volumic concentration.

Fig. 11. Time and space averaged profiles.
solid line: DVM; squares : Experiment of Villaret and Latteux (1992).

As a direct consequence of these discrepancies, the computed fluxes profiles (Fig. 12) exhibit a completely different pattern from data. At higher elevations where the concentration is overestimated, F_s and F_c exhibit maxima, while at lower levels where a return flow is predicted, fluxes disagree in amplitude and direction.

Villaret and Latteux (1992) computed Q_s from the fluxes profiles, Q_t from sand budget and Q_b by subtraction. They used a constant extrapolation of the fluxes from the last measurement point (y_c/L_r=0.18) down to the crest level (y_c=0) and then performed a depth-integration. The same Eulerian method is used here. As the flux F_s is small in the near-bed layer, the two methods for obtaining Q_s give similar results (Table 3). Nevertheless, the rather close agreement with data is not meaningful when the discrepancies in fluxes profiles are considered. The bed load is underpredicted and accounts for only 10% of the total transport compared to roughly 20% in the experiment.

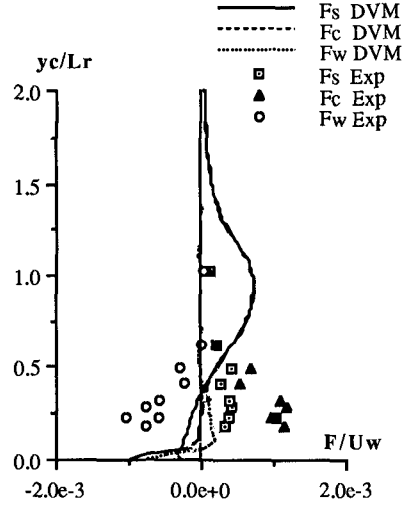

Fig. 12. Non-dimensional horizontal suspended sediment fluxes profiles. Experiment of Villaret and Latteux (1992).

$Q/L_r/U_w*10^{-4}$	*DVM*	*Exp*	*Ratio*
Bed load			
Q_b	0.2	0.5	0.4
Suspended load (Eul)			
Q_s	2.1	1.6	1.3
Q_c	2.0	2.6	0.8
Q_w	0.1	-1.0	-0.1
Suspended load (Lag)			
Q_s	2.0	*	*
Total load			
Q_t	2.2	2.1	1.1

Table 3. Non-dimensional transport rates. Experiment of Villaret and Latteux (1992). (: unavailable)*

DISCUSSION OF THE RESULTS AND CONCLUSIONS

A numerical model based on a discrete vortex approach has been developed to study flow and sediment processes over rippled beds. It has been tested for a representative experiment in clear oscillatory flow and three different configurations where the free stream asymmetry induces a transport of sand in the near-bed region.

As far as hydrodynamics are concerned, the model provides a consistent prediction of the processes in the near-bed layer dominated by coherent vorticity structures. For the wave-alone case, the experiment of Ranasoma (1992) with fixed ripples has been used as a validating test. The model is able to describe rather accurately the mechanisms of generation, ejection and convection of vortices. For

combined waves and current, the model predicts a two-layer flow structure in accordance with the experimental data of Murray (1992) in tunnel.

The consistent qualitative picture of suspension processes and the good agreement of concentration profiles found by Hansen *et al* (1994) for the wave-alone case are extended here to the case of asymmetric waves and combined waves and current in tunnel. Especially, the large-scale mixing resulting from vortex shedding generates a rather uniform concentration in the ripple-influenced near-bed layer.

Regarding suspended sediment transport, detailed flux profiles provide much more information than depth-integrated transport rates. The particularity of such unsteady flows is to give rise to a wave flux in addition to the current flux. The total suspended sediment flux is then the sum of these two contributions. The current flux is always in the direction of the local current (negative for asymmetrical wave and positive for combined waves and current) whereas the wave flux opposes the direction of the maximum free stream velocity at most levels. This results from the convection of sand-laden vortices generated during the positive flow, shed into the flow at reversal and convected backwards during the negative flow. In the near-bed region, the wave flux reverses and becomes strongly onshore. This behaviour is thought to be the result of the larger amount of sand picked up from the crest during the positive flow. The fluxes data of Murray (1992) provides a successful quantitative comparison for the vortex-dominated region but no data is available to understand clearly near-bed mechanisms.

The evaluation of suspended sediment transport rates has proven the importance of the choice of the lower limit for depth-integration when the fluxes exhibit large increases close to the bed.

A discrepancy between model results and experimental data arises for combined waves and current in a flume (Villaret and Latteux, 1992). Progressive waves induce vertical velocities and a drift positive at the bottom and negative above. The absence of this physical feature in the modelling results in a conspicuous two-layer structure with a large underestima tion of the horizontal velocity and a steep concentration profile in the near-bed region, whereas in the experiment the wave drift produces much more gradual profiles. The resulting computed fluxes disagree with experiment not only in magnitude but also in direction. This simulation demonstrates the need to include in the model the effect of wave propagation.

In such unsteady flows, the assumption of a steady-state ripple can be discussed. Indeed the ripple deforms locally during the wave cycle : a small volume of sand moves back and forth in the crest region and forms at each half-cycle a small cliff downstream of the crest which disappears at flow reversal (Sleath, 1982). In the simulations with sediment, the selected shape, "smoothed parabolic", is representative of the experimental bed shape (Fredsøe and Deigaard, 1992) and changing the length of the smoothed crest region has only a small influence on bottom processes. It appears from experiments that the bed is less affected by the superposition of a current on sine waves than by the wave asymmetry. Therefore, symmetric ripples have been used for combined waves and current simulations. Beside its stationary shape, the migration of the ripple is neglected based upon experiments. Nevertheless, the large increase in the computed wave flux close to the bed could be partly due to this unrepresented characteristics.

As a general conclusion, the study has demonstrated the ability of the model to replicate hydrodynamical and sediment mechanisms when the water motion induced by waves can be reckoned as oscillatory.

Acknowledgements.

This work was founded jointly by the Danish Technical Research Council under the program "Marin Teknik", the G8 Coastal Morphodynamics program under EC contract MAST2-CT92-0027 and by the French Sea State Secretary S.T.C.P.M.V.N.

Appendix : Experimental conditions.

Experiment Facility	*Motion*	*Test*	U_w *(cm/s)*	$U_w/\hat{U}$	T *(s)*	a/L_r	U_c/U_w	H_r/L_r	$Re=U_wL_r/\nu$	d_{50} *(mm)*
Ranasoma (92) Oscillatory rig	W	2A	20.3	0.5	2.41	0.78	-	0.18	18000	0.41
Sato (86) Tunnel	Asym W	S3-03	39.3	0.63	4.0	1.60	-	0.16	48000	0.18
		C2-12	40.6	0.72	3.0	1.30	-	0.14	38000	0.18
		C3-37	67.0	0.83	5.0	1.25	-	0.15	120000	0.18
Murray (92) Tunnel	W+C	WCS1	41.3	0.5	10.0	6.57	0.38	0.15	36000	0.14
Villaret Latteux (92) Flume	W+C	40	34.0	0.5	2.0	1.91	0.43	0.12	36800	0.07

References.

Block, M.E. (1994). Wave generated flow over sand ripples and the resulting entrainment and suspension of sediment. *PhD Thesis. Univ. Col. North Wales.*

Blondeaux, P. and G. Vittori (1990). Oscillatory flow and sediment motion above a rippled bed. *Proc. 22nd ICCE*, pp 2186-2199.

Fredsøe, J. (1984). Turbulent boundary layer in wave and current motion. *J. Hydr. Eng., ASCE,* 110(8), pp 1103-1120.

Fredsøe, J. and R. Deigaard (1992). Mechanics of coastal sediment transport. *Advanced Series on Ocean Engineering.* Vol. 3. World Scientific.

Hansen, E. A., J. Fredsøe and R. Deigaard (1994). Distribution of suspended sediment over wave-generated ripples. *J. Waterway, Port, Coastal and Ocean Eng., ASCE*, 120(1), pp 37-55.

Huynh Thanh S. (1990). Etude numérique de la couche limite turbulente oscillatoire générée par l'interaction houle-courant en zone côtière. *PhD Thesis. INPG Grenoble.*

Longuet-Higgins M. S. (1981). Oscillating flow over steep sand ripples. *J. Fluid Mech.*, 107, pp 1-35.

Murray P. B. (1992). Sediment pick-up in wave-current flow. *PhD Thesis. Univ. Col. North Wales.*

Ranasoma K. 1. M. (1992). Measurements in combined oscillatory and steady flow over rippled beds. *PhD Thesis. Cambridge.*

Sato S. , N. Mimura and A. Watanabe (1984). Oscillatory boundary layer flow over rippled beds. *Proc. 19th ICCE,* pp 2293-2309.

Sato, S. and K. Horikawa (1986). Laboratory study on sand transport over ripples due to asymmetric oscillatory flows. *Proc. 20th ICCE*, pp 1481-1495.

Sleath J. F. A. (1982). The suspension of sand by waves. *J. Hydr. Res.*, 20(5), pp 439-452.

Tsujimoto G., N. Hayakawa, M. Ichiyama, Y. Fukushima and Y. Nakamura (1991). A study on suspended concentration and sediment transport mechanism over rippled sand bed using a turbulence model. *Coastal. Eng. Japan,* 34(2), pp 177-189.

Villaret, C. and B. Latteux (1992). Transport of fine sand by combined waves and current : an experimantal study. *Proc. 23rd ICCE,* pp 2500-2512.

Vincent C. E. and M. O. Green (1990). Field measurements of the suspended sand concentration profiles and fluxes and of the resuspension coefficient gammma0 over a rippled bed. *J. Geophys. Res.*, 95(C7), pp 11591-11601.

Wiberg P. L. and C. K. Harris(1994). Ripple geometry in wave-dominated environments. *J. Geophys. Res.*, 99(c1), pp 775-789.

Zyserman, J. and J. Fredsøe (1994). Data analysis of bed concentration of suspended sediment. *J. Hydr. Eng., ASCE,* vol 120(9), pp 1021-1042.